The Astrophysical Journal, 602:320–326, 2004 February 10

CESSATION OF X-RAY PULSATION OF GX 1+4

Wei Cui and Benjamin Smith
Department of Physics, Purdue University, West Lafayette, IN 47907; cui@physics.purdue.edu, smith110@physics.purdue.edu
Received 2003 May 5; accepted 2003 October 18

ABSTRACT

We report results from our weekly monitoring campaign on the X-ray pulsar GX 1+4 with the *Rossi X-Ray Timing Explorer* satellite. The spin-down trend of GX 1+4 was continuing, with the pulsar being at its longest period ever measured (about 138.7 s). At the late stage of the campaign, the source entered an extended faint state, during which its X-ray (2–60 keV) flux decreased significantly, to an average level of $\sim 3 \times 10^{-10}$ ergs cm^{-2} s^{-1}. It was highly variable in the faint state; the flux dropped to as low as $\sim 3 \times 10^{-11}$ ergs cm^{-2} s^{-1}. In several observations during this period, the X-ray pulsation became undetectable. We can therefore conservatively conclude that the pulsed fraction, which is normally $\gtrsim 70\%$ (peak-to-peak), must have decreased drastically in those cases. This is very similar to what was observed in GX 1+4 in 1996, when it became similarly faint in X-ray. In fact, the flux at which the cessation of X-ray pulsation first occurred is nearly the same as it was in 1996. We suggest that we have once again observed the propeller effect in GX 1+4, a phenomenon that is predicted by theoretical models of accreting X-ray pulsars.

Subject headings: accretion, accretion disks — pulsars: individual (GX 1+4) — X-rays: stars

1. INTRODUCTION

Accreting X-ray pulsars are neutron stars in a binary configuration. The X-ray emission of such a system is powered by the accretion of matter from the companion star onto the neutron star. Therefore, unlike their isolated counterparts, neutron stars in a binary configuration are strongly influenced by the mass accretion process.

In many cases, it is believed that an accretion disk is formed around the neutron star in an accreting pulsar. The disk is disrupted by the strong magnetic field of the neutron star at the magnetospheric radius, where plasmas in the disk are channeled to the polar regions of the star along the field lines, creating "hot spots" there. However, if the magnetospheric radius is larger than the corotation radius of the neutron star, the accreted matter hits the centrifugal barrier and is likely to be expelled from the system (Illarionov & Sunyaev 1975; Wang & Robertson 1985; Lovelace, Romanova, & Bisnovatyi-Kogan 1999; Bogovalov 2001). This phenomenon is often referred to as the propeller effect.

Observationally, the propeller effect may manifest itself directly in the cessation of pulsation of an accreting pulsar, when the mass accretion rate is sufficiently low (and thus the magnetosphere is sufficiently large). This was indeed first observed in two systems, GX 1+4 and GRO J1744−28 (Cui 1997), which possess contrasting magnetic properties. It was seen again recently, based on our monitoring observations of GX 1+4 during its transition to a rare X-ray–faint state (which was very similar to the 1996 episode; Cui 1997). In this paper, we present the new data. We show that the results obtained are in good agreement with those of previous measurements and thus provide additional support for the earlier interpretation.

2. OBSERVATIONS

We monitored GX 1+4 weekly with the *Rossi X-Ray Timing Explorer* (*RXTE*) over a 2 yr period (2001–2002). Typical observing times are 2–3 ks (roughly one *RXTE* orbit), although some longer observations were taken, in coordination with the *Chandra X-Ray Observatory*, following the triggering of a Target-of-Opportunity program. For this work, we will focus on the *RXTE* observations taken in 2002, when a transition to a faint state occurred. The results of the *Chandra* observation will be discussed elsewhere.

There are two detectors on board *RXTE* (Bradt, Rothschild, & Swank 1993), the Proportional Counter Array (PCA) and the High-Energy X-Ray Timing Experiment (HEXTE). The PCA consists of five nearly identical large-area proportional counter units (PCUs). It has a total collecting area of about 6500 cm^2 and covers a nominal energy range of 2–60 keV. The HEXTE has a total effective area of about 1600 cm^2 in two clusters. Each cluster contains four detectors, although one of the detectors lost its spectral capability very early in the mission. The HEXTE covers a wide energy range of about 15–250 keV, overlapping the PCA passband at low energies. Since the HEXTE clusters alternate between on-source and off-source fields, the effective exposure time (with dead time subtracted) is always much less than the actual observing time.

Operational constraints require that some PCUs be turned off. Which PCUs are turned off varies from observation to observation. In our case, the number of PCUs that were operational varied from two to five, with PCU 0 and PCU 2 remaining on throughout the entire campaign. Because PCU 0 has lost its front veto layer, which makes background estimation more uncertain, we chose PCU 2 as our "standard" detector to normalize the measured fluxes.

3. DATA REDUCTION AND ANALYSIS

We used the software package HEASOFT 5.2,[1] along with the associated calibration files and background models, to reduce the *RXTE* data for spectral analysis. Specifically, FTOOLS 5.2 was used to extract spectra, both from PCA data and HEXTE data, and XSPEC 11.2 was used for spectral modeling. For timing analysis, however, we used custom

[1] Additional information is available at http://heasarc.gsfc.nasa.gov/docs/software/lheasoft.

software developed at MIT. The software is mature and has been used by the all-sky monitor (ASM) team since the beginning of the mission. It was designed to work directly with raw packet data, instead of standard FITS files.

3.1. *X-Ray Spectral Analysis*

To minimize calibration uncertainties associated with the PCA response matrices, we limited ourselves to data from the first xenon layer of each PCU that was turned on during an observation. The trade-off is that we lost sensitivity to X-rays at energies roughly above 25 keV. We used the HEXTE data to constrain the higher energy portion of the X-ray spectra. It should be noted that cross flux-calibration between the PCA and the HEXTE remains an unresolved issue.[2] The effect was taken into account in joint PCA/HEXTE spectral fits by making the relative normalization of the detectors an additional free parameter (i.e., multiplying the model by a constant in XSPEC). This approach has been commonly adopted (e.g., Coburn et al. 2002). Moreover, we chose to extract a spectrum from each PCU and each HEXTE cluster separately and to perform a global fit for each observation, while floating the relative normalization of each spectrum (with respect to PCU 2). This allowed us to also take into account more subtle differences in the effective areas of individual detectors. It also added flexibility in our dealing with the PCUs being turned on and off in the middle of an observation.

3.2. *X-Ray Timing Analysis*

To derive properties of the pulsed emission, we made a light curve for each observation from the *Standard 1* data, which has a time resolution of 1/8 s and covers the entire PCA passing band. The light curve was then barycenter-corrected and folded at trial periods close to the expected value (since the pulse period is not expected to vary significantly from week to week). At each trial period (P), we compute the following statistic (Leahy et al. 1983):

$$S = \sum_{i=1}^{N} \frac{(r_i - \bar{r})^2}{\bar{r}} t_i, \tag{1}$$

where N is the number of phase bins, r_i is the average count rate in phase bin i, t_i is the exposure time, and $\bar{r}$ is the overall average count rate. For this work, we chose $N = 19$ and the folding epoch to be MJD 52,466.0 (which is roughly at the middle of the monitoring campaign). In the absence of any periodic or secular variations, S follows the χ^2 distribution with $N-1$ degrees of freedom.

The true pulse period should correspond to where S peaks. To accurately locate the peak, we fitted the S-P curve with a parabolic function in a small region around the peak. It should be noted that we did not subtract background from the light curves, in order to preserve simple statistics (Leahy et al. 1983). However, any non-Gaussian variation in the background rate would invalidate the basis for S being χ^2 distributed. Fortunately, the effects of such variation seem to be quite small in our cases. A more serious complication arises from the fact that GX 1+4 itself exhibits aperiodic variations, as is evident from the presence of red noise in the power density spectrum (PDS; see Fig. 1 for an example). Therefore, S is *not* a χ^2_{N-1} random variable here, *even in the absence of a periodic signal*.

To reveal the underlying distribution of S, we constructed 100 simulated light curves for each observation, following a recipe in Timmer & König (1995). In order to derive analytic PDS models for the simulations, we excluded from a measured PDS a few bins around the harmonics of the pulsed signal (with the exact number of bins removed depending on the exposure time of the observation) and subtracted off the Poisson noise (see, e.g., Zhang et al. 1996 for a description of the procedure). We then fitted the PDS continuum with a simple power law, which, by eye, seems to describe the data adequately. Note that in all cases except one, the short duration of the observation does not allow the sufficient averaging of the PDS, over multiple segments or frequency bins, to quantify the low-frequency noise with meaningful Gaussian errors. Consequently, we chose to seek best fits by following the least-squares algorithm, as opposed to the usual χ^2 minimization. For the long observation ($\gtrsim$15 ks), we binned the raw PDS by a factor of 10 and performed a χ^2 fit. The best-fit model is quite similar to that from the least-squares fit, and the reduced χ^2 of the fit is about 1.5.

The best-fit model was used to simulate light curves for each observation. Each simulated light curve was then rerandomized bin by bin (by replacing the number of counts, n, in a time bin with a random number drawn from a Poisson distribution with a mean value of n) to simulate noise due to photon counting processes. The resulting simulated light curve was then folded at the measured pulse period to yield a value of S. Finally, we constructed a histogram of S for that observation (in the presence of red noise and photon counting noise alone). Figure 2 shows the 68% confidence regions of S for all observations, along with the values measured from actual data. The results are fairly robust with respect to modest amount of variation in the parameters of the input model. Clearly, the presence of red noise can seriously affect our ability in estimating the significance of the pulsed signal.

4. RESULTS

Figure 3 shows the flux history of GX 1+4 in 2002. The source was quite bright at the beginning of the year and was

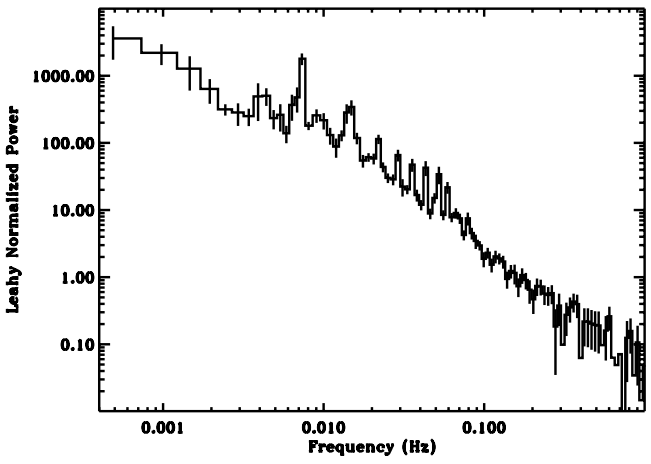

FIG. 1.—Sample power density spectrum of GX 1+4. The spectrum was made with data from the long observation taken on 2002 August 6 05:50:00–14:30:00 (UT). The harmonics of the pulsed signal are clearly visible. Note the presence of strong red noise.

[2] Additional information is available at http://lheawww.gsfc.nasa.gov/docs/xray/xte/crosscal.

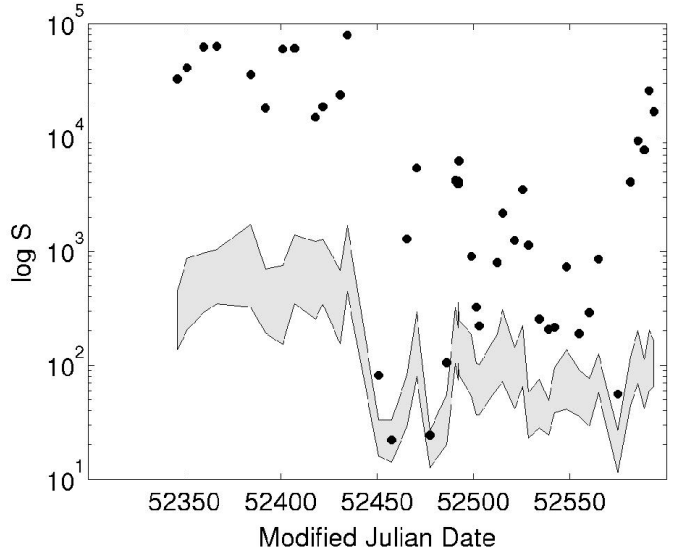

FIG. 2.—Epoch-folding statistics. The shaded area represents 68% intervals of the statistic, derived from simulations (see text), when no pulsed signal is present. The actual measured values are shown by filled circles.

seen to make a transition to a faint state in mid-June. The average flux is roughly an order of magnitude lower in the faint state than in the bright state, although it varies significantly in both states. The minimum flux measured is about another order of magnitude lower, reaching $\sim 3 \times 10^{-11}$ ergs cm^{-2} s^{-1}.

Toward the end of the year, GX 1+4 started to climb out of the faint state, as its timing and spectral properties gradually revert to those of the bright state (see discussions below). Unfortunately, our monitoring of the source was terminated too soon to cover the entire transition because of the proximity of the Sun to the source.

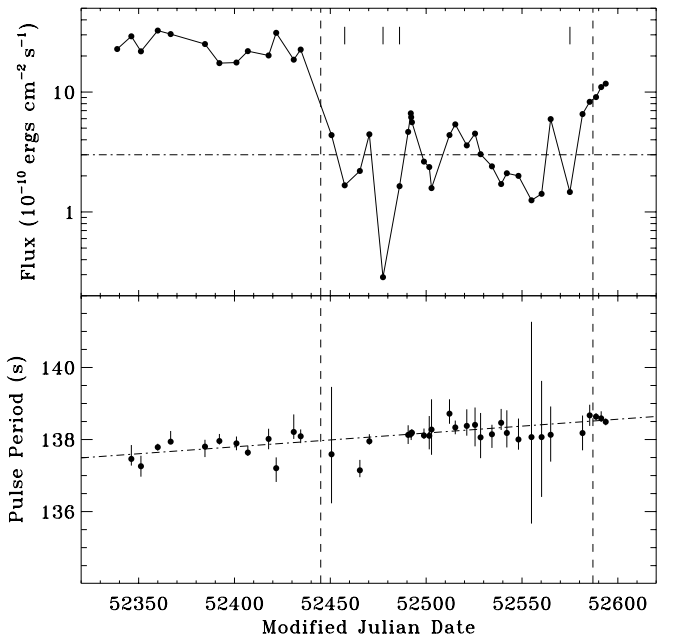

FIG. 3.—Measured X-ray fluxes and pulse periods of GX 1+4 in 2002. *Top*: Fluxes were measured in the 2–60 keV band, with negligibly small error bars; the vertical bars at the top indicate observations in which X-ray pulsation was not detected; the dot-dashed line shows the average flux of the source in the faint state. *Bottom*: Error bars on the pulse periods were derived from simulations and represent 68% confidence intervals; the dot-dashed line shows the best-fit spin-down trend. The boundaries of the faint state are crudely drawn with dashed lines. For reference, MJD 52,440 corresponds to 2002 June 15.

4.1. *Pulse Period and Pulse Fraction*

X-ray pulsation is detected with high significance in all but four cases in the faint state. Figure 4 (*top*) shows the *S-P* curve for one of the latter cases, which is basically flat. For comparison, we also show in the figure results for an adjacent observation (taken about a week earlier), in which the pulsation is clearly detected. The measured pulse periods (from the PCA data) are also shown in Figure 3. Note that no period is shown for the first observation, because it could not be reliably determined because of the very short exposure time of the observation (less than four pulse cycles). Although error bars are quite large in many cases (especially during the faint state), the spin-down trend can be seen from the figure. The best-fit spin-down rate is 4.4×10^{-8} s s^{-1}, which is less than half of the BATSE average (Bildsten et al. 1997). The source reached a pulse period of $\sim$138.7 s, the largest that has ever been measured.

There are two sources that contribute to the uncertainty in measuring the pulse period: one is associated with the epoch-folding technique, and the other is due to the presence of red noise. The former is well understood (see Larsson 1996), and we found that it was much smaller than the latter in all cases. We quantified the latter with simulations in the following manner. We added the observed pulsed signal to the simulated light curves (see § 3.2) for each of the observations in which the pulsation was detected with high significance. We then derived pulse periods from the new simulated light curves through the same epoch-folding procedure. A histogram of pulse periods was constructed in the end, and the 68% confidence region was determined. Therefore, the error bars have included the effects of intrinsic red noise of the source as well as of statistical fluctuations. We caution, however, that the reliability of the simulations depends sensitively on the accuracy of the input PDS model that we derived from the data.

The observed pulse profile varies significantly from observation to observation (i.e., over a timescale of days), much more so in the faint state. A thumbnail collection of pulse profiles are shown in Figure 5. The profiles were derived by folding light curves (2–60 keV) with reference to the same epoch (MJD 52,466.0), using the best-fit periods and period derivative (see Fig. 3). A feature that is common to a majority of the cases is the presence of a sharp dip in the pulse profile. The dips seem to occur at difference pulse phases. To be more certain about it, we experimented with deriving a phase coherence solution that connects the occurrence times of the dips, assuming they occur at a *constant* phase. In general, the pulse phase can be expressed as

$$\phi(t) = \phi(t_0) + \nu_0(t - t_0) + \tfrac{1}{2}\dot{\nu}_0(t - t_0)^2 + \tfrac{1}{6}\ddot{\nu}_0(t - t_0)^3 + \cdots,$$

where t_0 is the reference epoch, and ν_0, $\dot{\nu}_0$, and $\ddot{\nu}_0$ are the pulse frequency ($\equiv 1/P_0$), its first and second derivatives at $t = t_0$, respectively. We started by breaking the longest observation (at MJD 52,492) into six shorter segments. We folded the light curve of each segment and computed the time of the dip from the folded pulse profile. We did the same for two neighboring observations that were made about 1 week before and after the long observation. We were able to derive a timing solution (up to $\ddot{\nu}_0$) based on these data points. We then extended the time interval by adding one data point at a time and repeated the

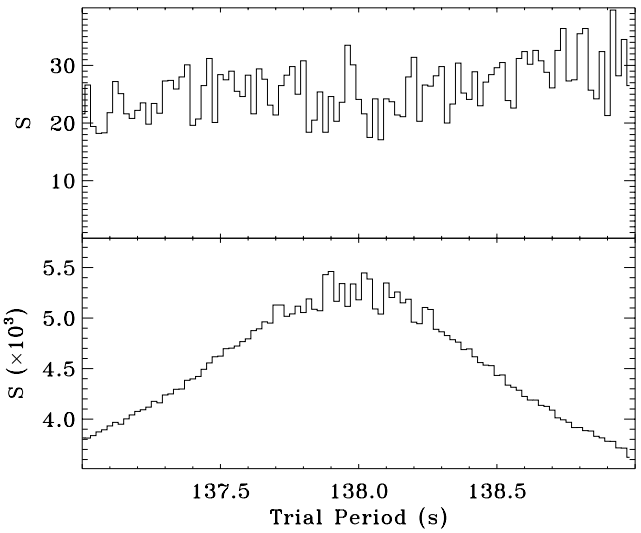

FIG. 4.—Folding statistics at various trial periods for two observations about 1 week apart. The observations took place on 2002 July 15 and 21, respectively. No pulsation can be detected in the latter (*top*), while it is clearly present in the other (*bottom*).

procedure. However, we failed to find a global phase coherent solution. Figure 6 shows that the residuals after the best-fit model have been subtracted from the data. This result seems to suggest that the dip does not always occur at a fixed pulse phase, although we cannot rule out the possibility that it is caused by nonvanishing higher order period derivatives. Similar dips were seen previously (e.g., Dotani et al. 1989; Giles et al. 2000) and were interpreted as being due to either obstruction of the "hot spot" by the accretion column (e.g., Giles et al. 2000; Galloway et al. 2001) or resonance scattering of photons in the accretion column above the magnetic pole (Dotani et al. 1989). However, it would seem difficult for either scenario to explain why the dip does not occur at a constant pulse phase.

As is obvious from Figure 5, when GX 1+4 is relatively bright (the first 13 observations as well as the last few; see Fig. 3), its X-ray flux is strongly modulated. When the source reaches the faint state, the pulsed fraction is significantly reduced and the pulse profile takes on drastically different forms. In four of the cases (see Fig. 5), the folded light curves show no sign of periodic modulation. It should be kept in mind that GX 1+4 is known to exhibit red noise in its PDS (see Fig. 1 for an example). Consequently, much of the variation seen in the folded light curves can be caused by variations of the source that are associated with the red noise. To illustrate this point, we show in Figure 7 a comparison between a measured light curve and a simulated light curve for one of the observations in which no pulsation was detected. The non-Gaussian variation in the former can therefore be fully accounted for by the presence of red noise alone. We also investigated, with *goodXenon* data, the possibility that the signal might be detected only at higher energies for these cases. We constructed light curves that only include photons above roughly 7 keV and repeated the period-search procedure.

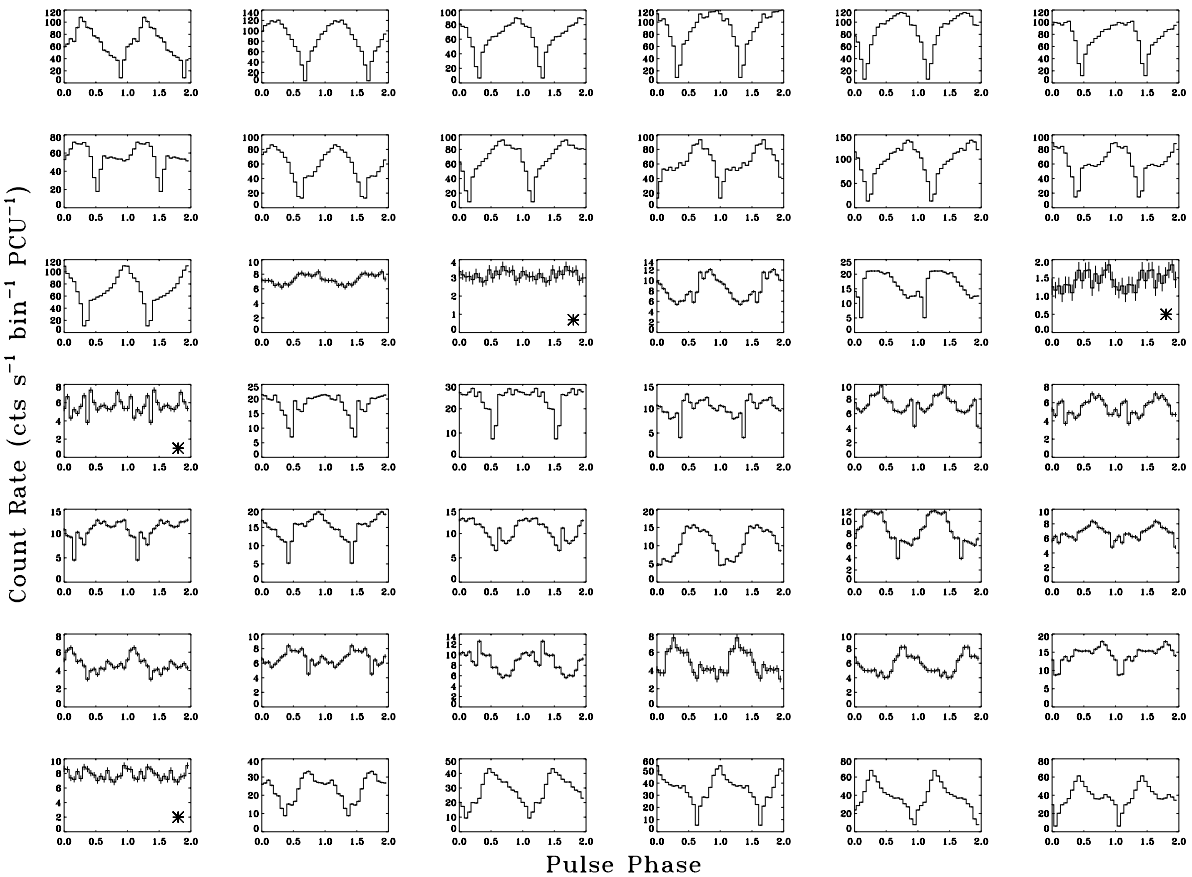

FIG. 5.—Observed pulse profiles of GX 1+4 in chronological order, from left to right and top to bottom. The average background rate has been subtracted in each case. Note that no pulsation is apparent in four of the observations (marked by asterisks).

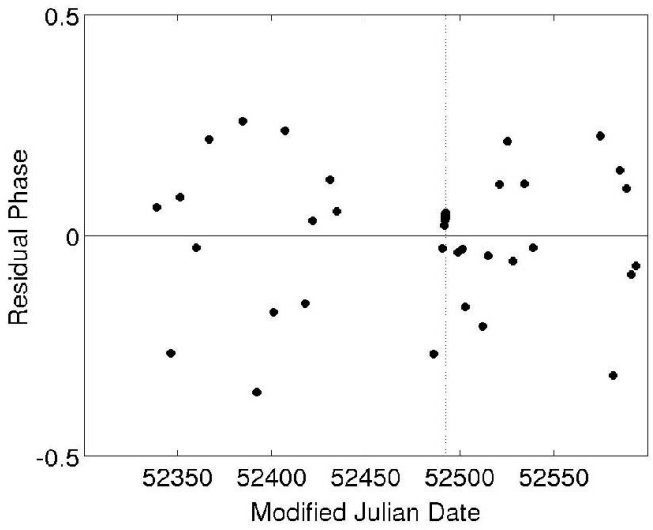

FIG. 6.—Dip occurrence time residuals with the best-fit timing model (up to $\ddot{\nu}$) subtracted. Error bars are negligible on this scale. The dotted line indicates where the reference epoch (t_0) is located (see text). Note that not all observations clearly show the presence of a dip in the folded pulse profile (see Fig. 5).

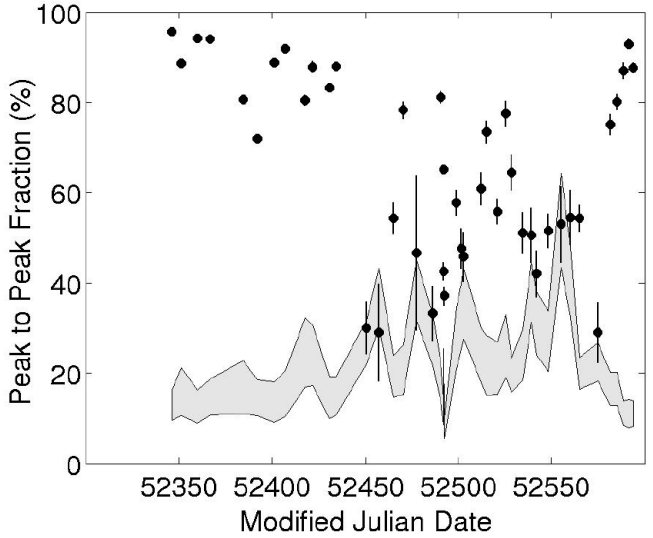

FIG. 8.—Fractional peak-to-peak pulsed fraction. The filled circles show the measured values. The shaded region represents 68% intervals of the pulsed fraction, derived from simulations, when no pulsed signal is present.

No pulsation was detected. When the pulsation is not detected, the flux of GX 1+4 always seems to be $\lesssim 2 \times 10^{-10}$ ergs cm^{-2} s^{-1}. On the other hand, in a few other cases, the flux of the source falls below that threshold, yet the pulsation is detected with high significance. Therefore, the phenomenology is not simple.

To measure the amplitude of the pulsed signal, we defined the fractional peak-to-peak pulsed fraction as $f_{\rm pp} \equiv (F_{\rm max} - F_{\rm min})/F_{\rm max}$ and computed it for each observation. The results are shown in Figure 8. Of course, the pulsed fraction thus defined is not expected to be zero, even in the absence of any pulsed signal, because of statistical fluctuations and aperiodic variabilities. The results from simulations were again used to quantify the effects. Such "baseline" values of the pulsed fraction are shown in Figure 8. Note that the pulsed fraction does not stand above the baseline in some cases, even though the pulsation is clearly detected. This is due to the combination of uncertainties in the simulation, small pulsed fraction, and poor statistics of the data.

4.2. *Spectral Characteristics*

The X-ray spectrum of GX 1+4 can be described by a model that consists of a cutoff power law and a Gaussian function. Also included in the model is the absorption along the line of sight. The observed continuum is therefore typical of accreting X-ray pulsars (White, Swank, & Holt 1983). The Gaussian component is needed to mimic the strong iron Kα line at $\sim$6.4 keV, which is known to be present in the X-ray spectrum of GX 1+4 (Kotani et al. 1999). This is the same model as the one that was adopted to study GX 1+4 during its 1996 transition to the faint state (Cui 1997) and thus facilitates direct comparisons of the results.

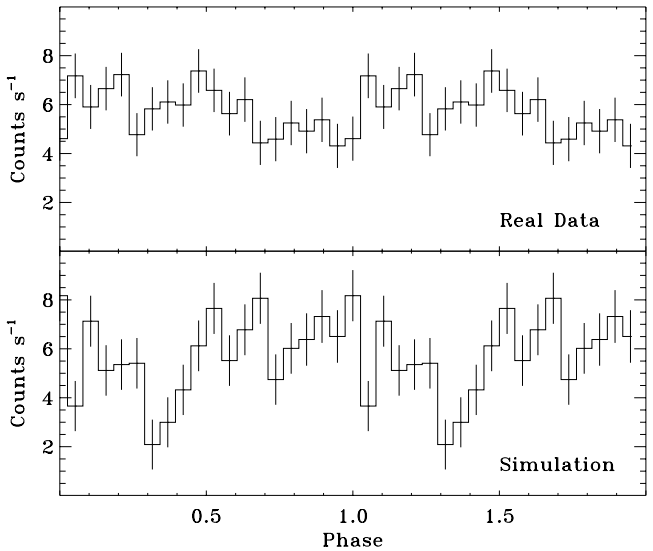

FIG. 7.—Comparison between the measured (folded) light curve and a simulated light curve for the same observation. No pulsed signal was included in the PDS model for the simulations. The "features" in the light curves are therefore purely due to the presence of red noise.

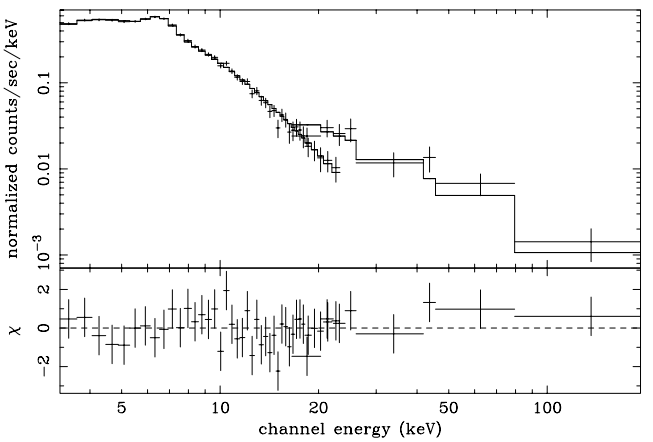

FIG. 9.—Composite X-ray spectrum of GX 1+4 in the faint state. The spectrum was derived by combining data from those observations that show no evidence of X-ray pulsation. The solid histogram shows the best-fit power-law model (which also includes interstellar absorption and an iron Kα line). Note that the spectrum extends beyond 100 keV, showing no evidence of rolling over.

To account for residual calibration uncertainties, we followed the usual practice of including a 1% systematic error in the analyses. The fits are quite satisfactory, with the reduced χ^2 values around 1, except for a few cases at the beginning of the monitoring campaign in which the source was bright. Even in the latter cases, the reduced χ^2 values are never more than $\sim$1.7, with deviations residing mostly at the lowest energies, where the PCA calibration is less certain.

When it is bright, GX 1+4 shows little intrinsic spectral variability. The measured photon index falls in a narrow range of 1.1–1.3, the exponential cutoff energy remains roughly at 8 keV, and the *e*-folding varies in the range of 28–40 keV. It is interesting to note that similar spectral characteristics were observed of the source during the last three observations, indicating the emergence of GX 1+4 from the faint state.

In contrast, the spectral properties of GX 1+4 appear to vary significantly in the faint state, on a timescale of days. Here, the photon index varies over a wide range of 0.2–2.0, with no apparent correlation with the measured flux. The spectrum of the source is the steepest in cases in which the pulsation is unmeasurable. In most cases, the spectrum rolls over at energies between 6 and 13 keV, with the *e*-folding energy in the range of 11–45 keV. However, no spectral rollover is observed when the pulsation ceases. To illustrate the effect, we made a composite spectrum by combining data from the four observations in which no pulsation is detected in order to achieve sufficient statistics at high energies. Figure 9 shows the spectrum, along with the best-fit model and the residuals. The presence of an iron Kα line is apparent; the continuum extends beyond 100 keV, following a simple power law with a photon index of roughly 1.6. To avoid divergence in overall luminosity, therefore, the spectrum must roll over at some energy, perhaps much beyond the HEXTE passing band. Very similar spectral variabilities were observed during the transition to a faint state in 1996 (Cui 1997).

The inferred hydrogen column density varies in the ranges of 4–9 and $(3-19)\times10^{22}$ cm^{-2} for the bright state and faint state, respectively. It is not as well (sometimes poorly) constrained in the latter case because of poorer statistics. These results are again comparable to those obtained previously (Cui 1997). The variability might be related to the changing physical conditions in the wind of the M giant companion star.

5. DISCUSSION

In this work, we have presented evidence for the cessation of X-ray pulsation of GX 1+4, when the source reached a low-flux state. While it is not technically feasible to rule out the presence of weak pulsation in such a case, we can at least conclude that the X-ray pulsed fraction must have decreased dramatically as the source made a transition from the bright state to the faint state. A similar phenomenon was observed previously (Cui 1997), but we have carried out a more detailed analysis in this work, taking into account the presence of intrinsic red noise with Monte Carlo simulations. We expect that the derived error bars on the pulsed fraction measurements, as well as significance estimates regarding the detection of pulsation, are more realistic. This is a point worth emphasizing, because much of the variability seen in a folded light curve could be attributed to the aperiodic secular variations of the source.

One thing that we do notice in this work is that there does not appear to be a fixed flux threshold below which the pulsation ceases, as one might naively expect from the propeller effect. This complicates the interpretation. Perhaps, in the faint state, GX 1+4 was close to the transition threshold and it flipped and flopped stochastically between the propeller state and the nonpropeller state. It might even be possible that there is some hysteresis associated with the transitions (see Fig. 2 of Lovelace et al. 1999). If the propeller phenomenon is indeed observed, it allows a direct estimation of the magnetic field in GX 1+4.

5.1. *Propeller Effect*

For accreting pulsars, the determination of magnetospheric radius is still uncertain theoretically (e.g., Ghosh & Lamb 1979; Wang 1996). The geometry of the magnetic field is often assumed to consist of closed field lines, threading the accretion disk (Ghosh & Lamb 1979). More recently, other field configurations (with open field lines originating in the accretion disk) have been investigated and may, in fact, be important for the propeller effect (e.g., Lovelace et al. 1999).

At the Alfvén radius, the magnetic pressure is balanced by the ram pressure of accreted matter. For a dipole field, the Alfvén radius is given by

$$r_{\rm A} = 5.2\times10^{8}\ {\rm cm}\, L_{\rm X,36}^{-2/7} B_{12}^{4/7} M_{1.4}^{1/7} R_6^{10/7} \qquad (2)$$

(Lamb, Pethick, & Pine 1973), where $L_{\rm X,36}$ is the bolometric X-ray luminosity in units of 10^{36} ergs s^{-1}, B_{12} is the field strength at the surface of the neutron star in units of 10^{12} G, and $M_{1.4}$ and R_6 are the mass and radius of the neutron star in units of 1.4 $M_\odot$ and 10^6 cm, respectively. The magnetospheric radius is probably a fraction of the Alfvén radius, $r_m = \eta r_{\rm A}$, where $0 < \eta \leq 1$ (e.g., Ghosh & Lamb 1979; Wang 1996; Lovelace et al. 1999).

The corotation radius, $r_{\rm co}$, is defined as the radius at which the Keplerian velocity is equal to the corotating velocity, $(GM/r_{\rm co})^{1/2} = \Omega r_{\rm co}$, where Ω is the angular velocity of the neutron star. Therefore, we have

$$r_{\rm co} = 4.5\times10^{9}\ {\rm cm}\, P_{138}^{2/3} M_{1.4}^{1/3}, \qquad (3)$$

where P_{138} is the rotation period of the neutron star in units of 138 s. The propeller effect takes place when $r_{\rm co} = r_m$. From equations (2) and (3), we find that the magnetic field strength is given by

$$B = 4.4\times10^{13}\ {\rm G}\, \eta^{-7/4} P_{138}^{7/6} L_{\rm X,36}^{1/2} M_{1.4}^{1/3} R_6^{-5/2}. \qquad (4)$$

For GX 1+4, the observed 2–60 keV X-ray fluxes are $(1.4-1.7)\times10^{-10}$ ergs cm^{-2} s^{-1}, for cases in which the X-ray pulsation is undetectable. Assuming a distance of 6 kpc (which is probably accurate to within a factor of 2; Chakrabarty & Roche 1997), the observed luminosities are $\sim7\times10^{35}$ ergs s^{-1}. Using this value in equation (4), we already have $B > 3.7\times10^{13}$ G. In some models, η can be much less than 1 (e.g., $\sim$0.3; Lovelace et al. 1999), so the inferred magnetic field might be an order of magnitude larger. We must also make bolometric corrections, taking into account absorption at low energies and spectral rollover at high energies, the latter of which is necessary to keep the integrated flux from diverging. While the low-energy correction is expected to be small ($\lesssim$30%), the high-energy correction can be quite large, depending on where the spectrum rolls over, given the relatively flat spectrum of the source. In extreme scenarios,

therefore, the magnetic field of GX 1+4 could reach the magnetar regime!

5.2. *Origin of the Persistent Emission in the Propeller State*

In the propeller regime, the accreted matter can no longer be channeled to the surface of the neutron star by the magnetic field. Instead, it might be accumulated at the magnetosphere and gradually build up a dense envelope around it. In this scenario, the matter might be accumulated preferentially near the direction of the rotation axis and be expelled along the perpendicular direction (Wang & Robertson 1985). In the process, the matter could be heated up to tens of millions of degrees and produce thermal bremsstrahlung radiation. However, the spectrum of such radiation should roll over exponentially at tens of keV, which we did not observe in the case of GX 1+4. Therefore, the observed persistent emission is unlikely to be of magnetospheric origin.

The propeller effect was also invoked to explain the large luminosity variation of 4U 0115+63 near its pariastron passage (Campana et al. 2001). It was argued that the emission from the accretion disk would be important in the propeller regime. However, in the case of GX 1+4, the inner edge of the disk would be quite far away from the neutron star in the propeller regime and thus be too cool to contribute much to the observed X-ray emission. Moreover, the observed X-ray spectrum of GX 1+4 is clearly not that of disk emission.

On the other hand, we know that GX 1+4 has an M giant companion star, which is expected to produce a relatively dense, slow stellar wind (Chakrabarty & Roche 1997). As the propelled matter plows into this wind at a velocity of the order of the escape velocity (Illarionov & Sunyaev 1975), $(2GM/r_{\rm co})^{1/2} \simeq 2000$ km s^{-1}, a strong shock might be formed. The shock could then produce a population of relativistic electrons via the first-order Fermi process. In this scenario, the observed persistent emission could simply be attributed to the synchrotron radiation of these electrons in the relatively strong magnetic field. The nonthermal nature of such emission is consistent with the lack of spectral rollover in the propeller state. This emission mechanism is thought to be responsible for the unpulsed X-ray emission observed from the Be binary pulsar system PSR B1259−63 near periastron (Grove et al. 1995).

One potential complication might arise from the fact that GX 1+4 is located in the crowded Galactic center region. Since the flux of the source is quite low in the faint state, the issue of source confusion needs to be addressed. This can directly affect the derivation of pulsed fraction. More seriously, however, we need to be certain that GX 1+4 was detected at all in the faint state. We searched the existing X-ray catalogs for known sources within a 1° radius circle around GX 1+4 and only found a number of very faint *ROSAT* sources, some of which might be transient in nature. For a Crab-like spectrum, the fluxes of these sources are all below 10^{-13} ergs cm^{-2} s^{-1}. This is consistent with results from our deep *Chandra* observation (with an exposure time of 60 ks) in the faint state: over the entire field of view ($8\farcm3 \times 50\farcm6$ with the spectroscopic array), we detected only two very faint sources whose fluxes are more than 2 orders of magnitude lower than the faint-state flux of GX 1+4. Moreover, the fact that we did also detect pulsation at comparable fluxes is reassuring. The presence of the characteristic iron Kα line in all observations adds another piece of evidence that the source never completely turned off its X-ray emission during our campaign.

We wish to thank Duncan Galloway for many helpful discussions and John Finley for his advice on pulse timing and comments on the manuscript. This research has made use of data obtained through the High Energy Astrophysics Science Archive Research Center Online Service (HEASARC), provided by the NASA/Goddard Space Flight Center. We gratefully acknowledge financial support from NASA through an Long Term Space Astrophysics Program (LTSA) grant (NAG5-9998) and a *Chandra* grant (GO2-3052X).

REFERENCES

Bildsten, L., et al. 1997, ApJS, 113, 367
Bogovalov, S. V. 2001, Astron. Lett., 27, 176
Bradt, H. V., Rothschild, R. E., & Swank, J. H. 1993, A&AS, 97, 355
Campana, S., et al. 2001, ApJ, 561, 924
Chakrabarty, D., & Roche, P. 1997, ApJ, 489, 254
Coburn, W., et al. 2002, ApJ, 580, 394
Cui, W. 1997, ApJ, 482, L163
Dotani, T., et al. 1989, PASJ, 41, 427
Galloway, D. K., Giles, A. B., Wu, K., & Greenhill, J. G. 2001, MNRAS, 325, 419
Ghosh, P., & Lamb, F. K. 1979, ApJ, 234, 296
Giles, A. B., Galloway, D. K., Greenhill, J. G., Storey, M. C., & Wilson, C. A. 2000, ApJ, 529, 447
Grove, J. E., et al. 1995, ApJ, 447, L113
Illarionov, A. F., & Sunyaev, R. A. 1975, A&A, 39, 185
Kotani, T., Dotani, T., Nagase, F., Greenhill, J. G., Pravdo, S. H., & Angelini, L. 1999, ApJ, 510, 369
Lamb, F. K., Pethick, C. J., & Pines, D. 1973, ApJ, 184, 271
Larsson, S. 1996, A&AS, 117, 197
Leahy, D. A., et al. 1983, ApJ, 266, 160
Lovelace, R. V. E., Romanova, M. M., & Bisnovatyi-Kogan, G. S. 1999, ApJ, 514, 368
Timmer, J., & König, M. 1995, A&A, 300, 707
Wang, Y.-M. 1996, ApJ, 465, L111
Wang, Y.-M., & Robertson, J. A. 1985, A&A, 151, 361
White, N. E., Swank, J. H., & Holt, S. S. 1983, ApJ, 270, 711
Zhang, W., Morgan, E. H., Jahoda, K., Swank, J. H., Strohmeyer, T. E., Jernigan, G., & Klein, R. I. 1996, ApJ, 469, L29